ISSN: 2644-2957
DOI: 10.33552/OJCAM.2026.09.000711
Online Journal of Complementary & Alternative Medicine
Iris Publishers

Research Article

Mathematical Model of Interstitial Fluid Flow During Acupuncture Needling by Lifting-Thrusting Manipulation

Manisha[1,2*], Sumit Kumar[2], V K Katiyar[3], and Pratibha[1]

[1]*Department of Mathematics, IIT Roorkee, Haridwar, Uttarakhand, India*
[2]*Government College for Women, Gurawara, Rewari, Haryana, India*
[3]*University of Patanjali, Haridwar, Uttarakhand, India*

***Corresponding author:** Manisha, Department of Mathematics, IIT Roorkee, Haridwar, Uttarakhand, India

Received Date: May 11, 2026
Published Date: June 11, 2026

Abstract

This study presents a numerical mathematical model of interstitial fluid flow at ST36 (stomach-36, Zusanli) acupoint in a porous biological tissue. The governing equations describe the flow using incompressible convective Brinkman equations with Kelvin-Voigt viscoelastic stress in cylindrical coordinates using an implicit finite difference scheme, which accounts for viscous diffusion, porous resistance and pressure-driven fluid transport. The effect of key physical parameters were examined, like Reynolds number, Darcy number, pressure gradient, and needle depth. The results show that a higher Darcy number results in higher fluid velocity, and a higher Reynolds number shows a stronger convective effect by keeping the flow in the viscous-dominated region. The pressure gradient is found to be the primary driving force for the fluid motion, while needle insertion depth variation produces local effects on velocity profiles near the needle. The proposed model provides a quantitative framework for understanding transport mechanisms of interstitial fluid associated with needle-based therapies.

Keywords: Acupuncture; Needling; Lifting-Thrusting; Interstitial Fluid Flow, etc.

Introduction

Human skin has layers of tissues and fat beneath it, including the epidermis, dermis, and hypodermis. Interstitial fluid is a gel-like fluid that circulates around the cells of tissues throughout the body, from the epidermis to the deeper organs. Interstitial fluid is part of the extracellular matrix and constitutes almost 20 per cent and is essential for the microcirculation of proteins and important minerals between blood vessels and the extracellular space [1, 2, 7]. Interstitial fluid is linked to lymphatic drainage, which helps return leaked plasma from the capillaries through the action of hydrostatic and osmotic pressure differences [1]. Interstitial fluid flow is driven by the pressure difference between the interstitium and the lymphatic system. Acupuncture is a well-known therapeutic process that involves the insertion and manipulation of needles at specific points on the body, known as acupuncture points or acupoints. Langevin et al. [3] found that these acupoints are interconnected by a network of channels, known as Meridians, spread throughout the body. To analyse the theory of Traditional Asian Medicine, i.e., the sensation of acupuncture needling (or the energy, Qi) flows through these meridians, which are anatomically present in the connective tissue plane. Additionally, [3] utilized ultrasound imaging on the human arm to confirm that there is a significant cellular change when needling is performed at acupoints. [15] reviewed the process of needling its mechanical processes, signal transmission due to needling and the precision of acupuncture treatment.

During needling at acupoints using various lifting-thrusting or rotation manipulation techniques, there is a deformation of local connective tissues or cells beneath the skin, which helps signal the sensation of needling. These local connective tissues are made up of mast cells, which are present in higher concentration at acupoints [4], and there are collagens present under the skin, which help in the transmission of information and energy through meridians [4]. [18] gives a mathematical model with lifting-thrusting manipulation technique and studies the importance of needling at acupoints. [16] quantitatively study that the increase in needle rotation angle and needling frequency increases the stimulation to the tissues and results in better treatment to the patients. Swartz and Fleury [1] modelled interstitial tissues as porous media and explained how Darcy's law is a continuum approximation of fluid flow in microscopic phenomena, and where the Brinkman equation can easily govern the flow patterns around solids (or cells) in the fluid-filled medium. [9] also studied interstitial fluid flow around solid bodies with the help of Brinkman's Law. In this study, the authors are considering the acupoint ST36 (stomach-36, Zusanli) for reference, which lies on the tibialis anterior muscle approximately four finger-breadths below the knee cap [10]. According to [11], the diameter of the acupuncture needle is about 0.22 mm, and the length is approximately 4 cm with an insertion depth of 2 to 3 cm [18]. Applying the convective Brinkman law along with the viscoelastic stress properties of the tissues. Brinkman law allows to consider no-slip boundary conditions. The authors aim to analyse changes in velocity patterns resulting from needle insertion at different depths within an interstitial fluid-filled domain. They scaled the domain to 1 x 1 cm2 where needle insertion depth ranges from 0.1 - 0.4 mm at the center.

Novelty of the work: The novelty of the present work lies in the development of the numerical model, which works in interstitial fluid flow that incorporates needle geometry with the incompressible convective Brinkman equation with viscoelastic stress from the Kelvin-Voigt model. The proposed approach provides a suitable method for studying interstitial fluid transport in porous biological tissues. The study helps therapists understand the acupuncture treatment mechanisms at interstitial fluid flow levels along with needle insertion depth analysis and the impact of pressure during needling.

Mathematical Model

This study analyses the flow of interstitial fluid as a Newtonian fluid in an axially symmetric domain containing a viscoelastic porous medium with a solid needle inserted during acupuncture needling, which has a cylindrical body with a conical tip [15, 17, 18] of varying depth δ. The tissues of the human body are assumed to be homogeneous, isotropic, and incompressible. The study examines the flow properties of interstitial fluid flowing in z (axial) direction, where r (radial) direction is perpendicular to z. The domain is cylindrical and axially ranging from $0 \le z \le L$ with an inserted acupuncture needle at the middle of the domain.

The shape of the needle [5, 17,18, 19] is

$$R_o = \begin{cases} R_o - H - \dfrac{2\delta}{L_o}\left(z - \left(d - \dfrac{L_o}{2}\right)\right), d - \dfrac{L_o}{2} \le z \le d \\ R_o - H - \dfrac{2\delta}{L_o}\left(d + \dfrac{L_o}{2} - z\right), d < z \le d + \dfrac{L_o}{2} \end{cases}$$

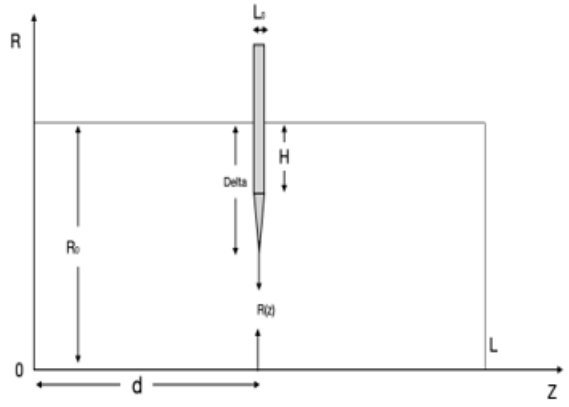

Figure 1: Geometry of the tissue as domain inserted with a solid needle of variable insertion depth delta (δ).

where $R0$ represents the radius of the domain, δ is the depth of the needle, which is inserted in the interstitial fluid matrix, d is mid midpoint of the domain where the needle is inserted in the radial direction, $L0$ is the length of the needle along the z axis. The fluid flow velocity is V = E$ur(r, \theta, z)$, $u\theta(r, \theta, z)$, $uz(r, \theta, z)$ H, and the flow is governed by the following continuity and incompressible convective Brinkman equation [6] along with Kelvin-Voigt Viscoelastic stress [12] (figure 1):

Continuity equation:

$$\nabla . \vec{u} = 0$$

Momentum equation:

$$\rho\left(\frac{\partial\vec{u}}{\partial t}+\left(\vec{u}.\nabla\right)\vec{u}\right)==-\nabla p+\mu\nabla^2\vec{u}-\frac{\vec{u}}{\kappa}\vec{u}+\nabla.\tau$$

Kelvin-Voigt viscoelastic stress:

$$\tau=Ge+\eta_s\frac{\partial e}{\partial t}$$

where $u\vec{K}=(u,v)$ is the velocity vector, p is the pressure, ρ is the density, μ is the dynamic viscosity, κ is the permeability of the porous medium, τ is the viscoelastic stress tensor, G is the shear modulus, ηs is the viscoelasticity coefficient of the solid matrix and, e is the strain rate tensor:

$$e_{ij}=\frac{1}{2}\left(\frac{\partial u_i}{\partial x_j}+\frac{\partial u_j}{\partial x_i}\right).$$

In a cylindrical coordinate system, the continuity equation:

$$\frac{1}{r}\frac{\partial}{\partial r}\left(ru_r\right)+\frac{\partial u_z}{\partial z}+\frac{1}{r}\frac{\partial u_\theta}{\partial\theta}=0$$

r – momentum equation:

$$\rho\left(\frac{\partial u_r}{\partial t}+u_r\frac{\partial u_r}{\partial r}+\frac{u_\theta}{r}\frac{\partial u_r}{\partial\theta}-\frac{u_\theta^2}{r}+u_z\frac{\partial u_r}{\partial z}\right)=-\frac{\partial p}{\partial r}+\mu\left[\frac{1}{r}\frac{\partial}{\partial r}\left(r\frac{\partial u_r}{r}\right)+\frac{1}{r^2}\frac{\partial^2u_r}{\partial\theta}-\frac{\partial u_r}{r}+\frac{\partial^2u_r}{\partial z^2}\right]$$
$$-\frac{u}{\kappa}u_r+\left(\frac{1}{r}\frac{\partial}{\partial r}\left(r\tau_{rr}\right)+\frac{1}{r}\frac{\partial\tau_{r\theta}}{\partial\theta}-\frac{\tau_{\theta\theta}}{r}+\frac{\partial\tau_{rz}}{\partial z}\right)$$

θ – momentum equation:

$$\rho\left(\frac{\partial u_\theta}{\partial t}+u_r\frac{\partial u_\theta}{\partial r}+\frac{u_\theta}{r}\frac{\partial u_\theta}{\partial\theta}+\frac{u_ru_\theta}{r}+u_z\frac{\partial u_\theta}{\partial z}\right)$$
$$=\mu\left[\frac{1}{r}\frac{\partial}{\partial r}\left(r\frac{\partial u_\theta}{\partial r}\right)+\frac{1}{r^2}\frac{\partial^2u_r}{\partial\theta^2}+\frac{2}{r^2}\frac{\partial u_r}{\partial\theta}-\frac{u_\theta}{r^2}+\frac{\partial^2u_r}{\partial z^2}\right]-\frac{u}{\kappa}u_\theta$$
$$+\left(\frac{1}{r^2}\frac{\partial}{\partial r}\left(r^2\tau_{r\theta}\right)+\frac{1}{r}\frac{\partial\tau_{r\theta\theta}}{\partial\theta}+\frac{\partial\tau_{r\theta}}{\partial z}\right)$$

z – momentum equation:

$$\rho\left(\frac{\partial u_z}{\partial t}+u_r\frac{\partial u_z}{\partial r}+\frac{u_\theta}{r}\frac{\partial u_z}{\partial\theta}+u_z\frac{\partial u_\theta}{\partial z}\right)=-\frac{\partial p}{\partial z}+u\left[\frac{1}{r}\frac{\partial}{\partial r}\left(r\frac{\partial u_z}{\partial r}\right)+\frac{1}{r^2}\frac{\partial^2u_z}{\partial\theta^2}+\frac{\partial^2u_z}{\partial z^2}\right]$$
$$-\frac{u}{\kappa}u_z+\left(\frac{1}{r}\frac{\partial}{\partial r}\left(r\tau_{rz}\right)+\frac{1}{r}\frac{\partial\tau_{r\theta z}}{\partial\theta}+\frac{\partial\tau_{zz}}{\partial z}\right).$$

Strain rate components are:

$$
\begin{aligned}
e_{rr} &= \frac{\partial u_r}{\partial r} \\
e_{\theta\theta} &= \frac{1}{r}\frac{\partial u_\theta}{\partial \theta} + \frac{u_r}{r} \\
e_{zz} &= \frac{\partial u_z}{\partial z} \\
e_{r\theta} &= \frac{1}{2}\left(\frac{1}{r}\frac{\partial u_r}{\partial \theta} + \frac{\partial u_\theta}{\partial r} - \frac{u_\theta}{r}\right) \\
e_{rz} &= \frac{1}{2}\left(\frac{\partial u_r}{\partial z} + \frac{\partial u_z}{\partial r}\right) \\
e_{\theta z} &= \frac{1}{2}\left(\frac{\partial u_\theta}{\partial z} + \frac{1}{r}\frac{\partial u_z}{\partial \theta}\right).
\end{aligned} \qquad (9)
$$

And stress components are

$$
\begin{aligned}
\tau_{rr} &= Ge_{rr} + \eta_s \frac{\partial e_{rr}}{\partial t} \\
\tau_{\theta\theta} &= Ge_{\theta\theta} + \eta_s \frac{\partial e_{\theta\theta}}{\partial t} \\
\tau_{zz} &= Ge_{zz} + \eta_s \frac{\partial e_{zz}}{\partial t} \\
\tau_{r\theta} &= Ge_{r\theta} + \eta_s \frac{\partial e_{r\theta}}{\partial t} \\
\tau_{rz} &= Ge_{rz} + \eta_s \frac{\partial e_{rz}}{\partial t} \\
\tau_{\theta z} &= Ge_{\theta z} + \eta_s \frac{\partial e_{\theta z}}{\partial t}
\end{aligned} \qquad (10)
$$

According to model assumptions, the fluid flow is axisymmetric; therefore, $\frac{\partial}{\partial \theta} = 0$ and $u_\theta = 0$, and in axial direction only, i.e. $u_r = 0$. The governing equations are simplified as

Continuity equation:

$$\frac{\partial u_z}{\partial z} = 0 \qquad (11)$$

r – momentum equation:

$$\frac{\partial p}{\partial r} = 0 \qquad (12)$$

z – momentum equation:

$$\rho\left(\frac{\partial u_z}{\partial t}\right) = \frac{\partial p}{\partial z} + \mu\left[\frac{1}{r}\frac{\partial}{\partial r}\left(r\frac{\partial u_z}{\partial r}\right)\right] - \frac{\mu}{k}u_z + \frac{1}{r}\frac{\partial}{\partial r}\left(r\tau_{rz}\right) \qquad (13)$$

As the fluid is considered to be Newtonian, therefore $\tau_{rz} = \frac{\eta_s}{2}\frac{\partial u_z}{\partial r}$.

z – momentum equation becomes

$$\rho\left(\frac{\partial u_z}{\partial t}\right) = -\frac{\partial p}{\partial z} + \mu\left[\frac{1}{r}\frac{\partial}{\partial r}\left(r\frac{\partial u_z}{\partial r}\right)\right] - \frac{\mu}{k}u_z + \frac{\eta_s}{2}\frac{\partial}{\partial t}\left[\frac{1}{r}\frac{\partial}{\partial r}\left(r\frac{\partial u_z}{\partial r}\right)\right] \qquad (14)$$

The initial and boundary conditions in dimensional form are as follows:

$uz = 0$ at $t = 0$, $\partial uz = 0$ at $r = R0$ *and* $R(z)$, $\partial uz = 0$ at ∂r $z = 0$ *and* $z = L$.

Non-Dimensionalisation: Considering $u_z = u$. To solve the equations numerically, non-dimensionalise the governing equations and needle geometry by scaling with the following parameters:

$$r^* = \frac{r}{R_0}, \quad z^* = \frac{z}{R_0}, \quad t^* = \frac{tU_0}{L_0}, \quad u^* = \frac{u}{U_0}, \quad p^* = \frac{p}{P_0}, \quad d^* = \frac{d}{R_0}, \quad H^* = \frac{H}{R_0},$$

$$\delta^* = \frac{\delta}{R_0}, \quad \mathrm{Re} = \frac{\rho U_0 R_0}{\mu}, \quad Da = \frac{k}{R_0^2}, \quad \beta = \frac{\eta_s U_0}{2\mu R_0}$$

Choose $P_0 = \frac{\mu U_0}{R_0}$,

where *Re* is the Reynolds number, *Da* is the Darcy number, and β measures the relative importance of viscoelastic stress to viscous stress. Momentum equation (after dropping asterisk):

$$\mathrm{Re}\left(\frac{\partial u}{\partial t}\right) = -\frac{\partial p}{\partial z} + \frac{1}{r}\frac{\partial}{\partial r}\left(r\frac{\partial u_z}{\partial r}\right) - \frac{1}{Da}u + \beta\frac{\partial}{\partial t}\left[\frac{1}{r}\frac{\partial}{\partial r}\left(r\frac{\partial u}{\partial r}\right)\right] \qquad (15)$$

To simplify the model, P_c, the pressure gradient is constant, which depends upon interstitial fluid pressure, osmotic pressure in the interstitial space and microvasculture, and hydraulic conductivity of capillary walls, also depending upon the difference between local interstitial pressure and pressure of the lymphatic system, lymphatic clearance rate [14]. Equation (15) becomes,

$$\mathrm{Re}\left(\frac{\partial u}{\partial t}\right) = -P_c + \left[\frac{1}{r}\frac{\partial}{\partial r}\left(r\frac{\partial u}{\partial r}\right)\right] - \frac{1}{Da}u + \beta\frac{\partial}{\partial t}\left[\frac{1}{r}\frac{\partial}{\partial r}\left(r\frac{\partial u}{\partial r}\right)\right] \qquad (16)$$

The initial and boundary conditions (after dropping the asterisk) are

$$u = 0 \text{ at } t = 0,$$

$$\frac{\partial u}{\partial r} = 0 \text{ at } r = 0,$$

$$\frac{\partial u}{\partial r} = 0 \quad r = R_0 \text{ and } R(z),$$

$$\frac{\partial u}{\partial z} = 0 \quad \text{at } z = 0 \text{ and } z = L.$$

Needle geometry in non-dimensional form

$$R(z) = \begin{cases} 1 - H - 2\delta\left(z - \left(d - \frac{1}{2}\right)\right), & d - \frac{1}{2} \le z \le d \\ 1 - H - 2\delta\left(d + \frac{1}{2} - z\right), & d < z \le d + \frac{1}{2} \\ 1 & ,\text{Otherwise} \end{cases}$$

The solution of the equation (15), along with the boundary conditions, is obtained with the help of the implicit finite difference method. The discretisation of the axial velocity is *un*, where u_i^n are space and time indices. The computational grids of the domain are as follows $r_i = i.\Delta r;\ i = 0,1,2,...L,\ t^n = n.\Delta t; \qquad n = 0,1,2,...,N.$ The partial derivatives are defined as

$$\frac{\partial u}{\partial r} \approx \frac{u_{i+1}^n - u_{i-1}^n}{2\Delta r}, \quad \frac{\partial u}{\partial t} \approx \frac{u_i^{n+1} - u_i^n}{\Delta t}, \quad \frac{\partial^2 u}{\partial r^2} \approx \frac{u_{i+1}^n - u_i^n + u_{i-1}^n}{(\Delta r)^2}.$$

$$L_i^n = \nabla^2 u \approx \frac{u_{i+1}^n - u_i^n + u_{i-1}^n}{(\Delta r)^2} + \frac{1}{r_i}\frac{u_{i+1}^n - u_{i-1}^n}{2\Delta r}, \frac{\partial}{\partial t}(\nabla^2 u) \approx \frac{L_i^{n+1} - L_i^n}{\Delta t}.$$

Equation (16) becomes:

$$\mathrm{Re}\,u_{i+1}^n - \beta L_i^{n+1} = \mathrm{Re}\,u_i^n - \beta L_i^n + \Delta t\left(-P_c + L_i^n - \frac{1}{Da}u_i^n\right)$$

$$a_i u_{i-1}^{n+1} + b_i u_i^{n+1} + c_i u_{i+1}^{n+1} = \mathrm{Re}\,u_i^n - \beta L_i^n + \Delta t\left(-P_c + L_i^n - \frac{1}{Da}u_i^n\right)$$

Where

$$a_i = -\beta\left(\frac{1}{\Delta r^2} - \frac{1}{2r_i\Delta r}\right), \ b_i = \mathrm{Re} + \frac{2\beta}{\Delta r^2}, \ c_i = -\beta\left(\frac{1}{\Delta r^2} + \frac{1}{2r_i\Delta r}\right)$$

Model Validation

The convergence and stability of a numerical solution are important, as one cannot find an exact solution to the partial differential equations. In this model, the stability of the implicit finite difference numerical scheme depends upon the step size and the time increment. In the present study, the accuracy of the results has been checked and found that the results converge to order 10^{-6} with the following stability:

$$dt < \frac{(dr)^2}{2}$$

Mesh independence analysis: To achieve predictive accuracy, a

mesh independence test is performed. A method used in numerical analysis to ensure that the results do not depend on the size and density of the grid of the domain. Authors compared the velocity at various axial points on grid sizes of 10 × 20, 20 × 40, 30×60, 40 × 80, 50 × 100 and 60 × 120.

Table 1: Fluid flow velocity on different grid sizes.

Grid ($dz \times dr$)	Velocity (u)
10 × 20	0.009992
20 × 40	0.009996
30 × 60	0.009996
40 × 80	0.009996
50 × 100	0.009996

Table 1 is prepared to show the velocity calculations on different grid refinements, and it is clarified in the table that there is 0.00000004 units of error in the velocities of grid 50 × 100 and 60 × 120. Therefore, the grid 50 × 100 is chosen to calculate numerical results.

Results and Discussion

In this study, the authors aimed to determine the flow patterns of the porous medium of interstitial fluid when an acupuncture needle is inserted perpendicular to the skin into the fluid matrix at an acupoint. Numerical simulations were performed to analyse the impact of needle depth and pressure gradient on velocity.

Effect of needle depth: In Figure 2, the velocity decreases as the radius increases and tends to zero on the needle surface as the needle depth (or delta) increases. From Figure 3(a)-(d), when the needle depth varies from 0.1 *mm* to 0.4 *mm*, the local flow field changes as the needle depth changes. When the depth is small, i.e. 0.1 *mm*, the velocity distribution is uniform throughout the domain, showing minimum disturbance in the interstitial fluid. As the needle penetrated deeper inside the tissue, the flow area reduced, which results in an increase in acceleration in the fluid flow pattern near the needle and higher velocity in the remaining area. This helps in easing the transportation of needling signals through the interstitial fluid. Figure 4 shows the velocity profiles when there are different pressure gradients. It shows that the velocity increases as the pressure gradient increases and drops to zero at the needle tip at an insertion depth of 0.2 *mm*.

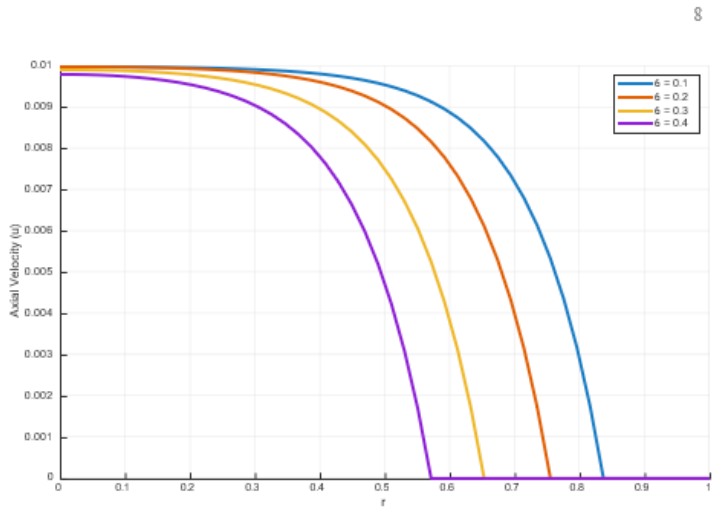

Figure 2: Velocity profiles near needle centre.

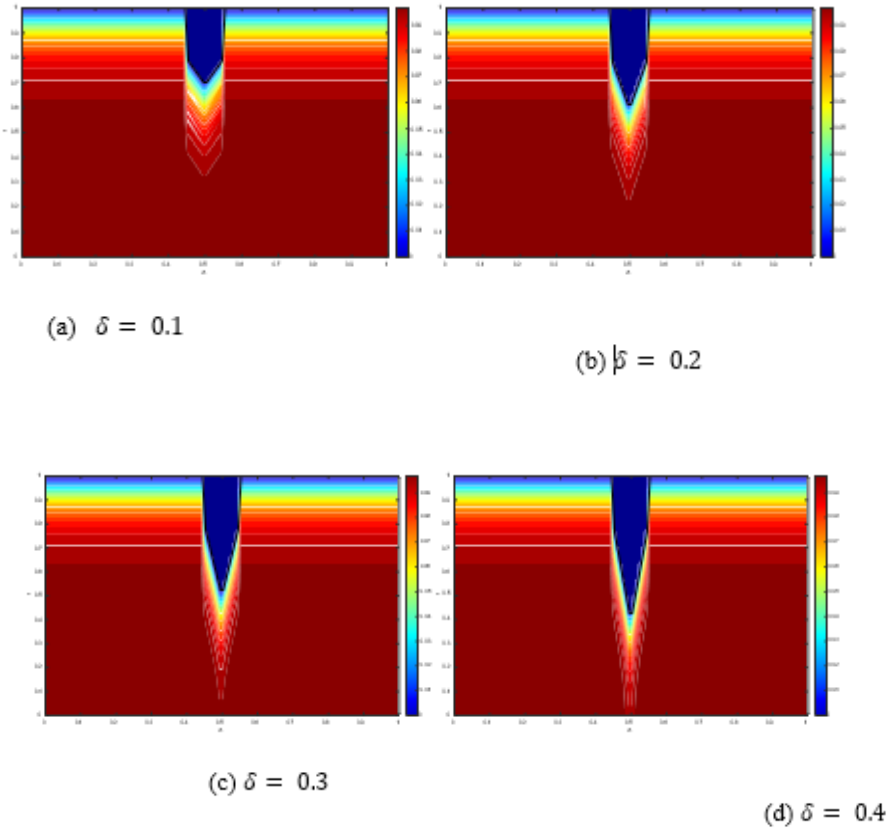

Figure 3: Interstitial flow induced by perpendicular needle insertion depth δ is 0.1, 0.2, 0.3, 0.4.

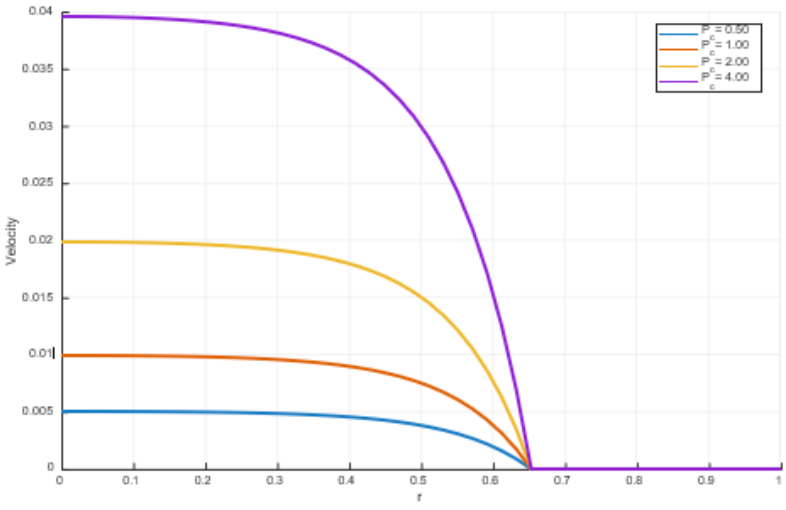

Figure 4: Axial velocity profiles with different pressure gradients.

Effect of pressure difference: Figure 4 shows the velocity profiles when there are different pressure gradients. It shows that the velocity increases as the pressure gradient increases and drops to zero at the needle tip at an insertion depth of 0.2 *mm*. In living tissues, a pressure gradient arises from vascular pressure difference, lymphatic drainage or mechanical stimulation caused by needle insertion. There is a proportional increase in pressure.

Effect of varying Reynolds number: In Figure 5, when there is variation in Reynolds number, Re = 0.015, 0.103, 0.208 [6], the velocity profiles show smooth variation in radial direction, showing maximum velocity in the inner region, and it reduces as radius increases. Such behavior is consistent with the viscous fluid-filled biological tissues. With an increase in Reynolds number, there is a reduction in velocity magnitude, which suggests that the inertial forces give additional resistance to the flow. The slight difference between the velocity curves with different Reynolds numbers explains the properties of interstitial fluid, where the flow creeps and shows that the flow is weakly dependent on Reynolds number.

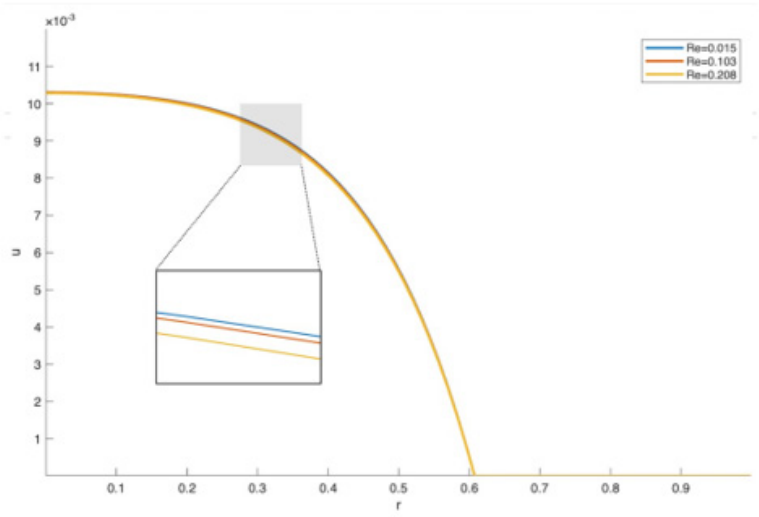

Figure 5: Axial velocity profiles with different Reynolds numbers.

Effect of varying Darcy number: Here, the Darcy number analyses the effect of permeability on interstitial fluid flow. In Figure 6, as the Darcy number increases from Da = 0.01, 0.040, 0.321, there is an increase in the velocity profiles, which shows that the larger Darcy number (or higher permeability) represents lower porous resistance to fluid motion that results in higher velocity magnitudes. In biological tissues, the Darcy number is directly related to extracellular matrix structure and porosity. Higher permeability is directly related to loose connective tissues and results in higher flow.

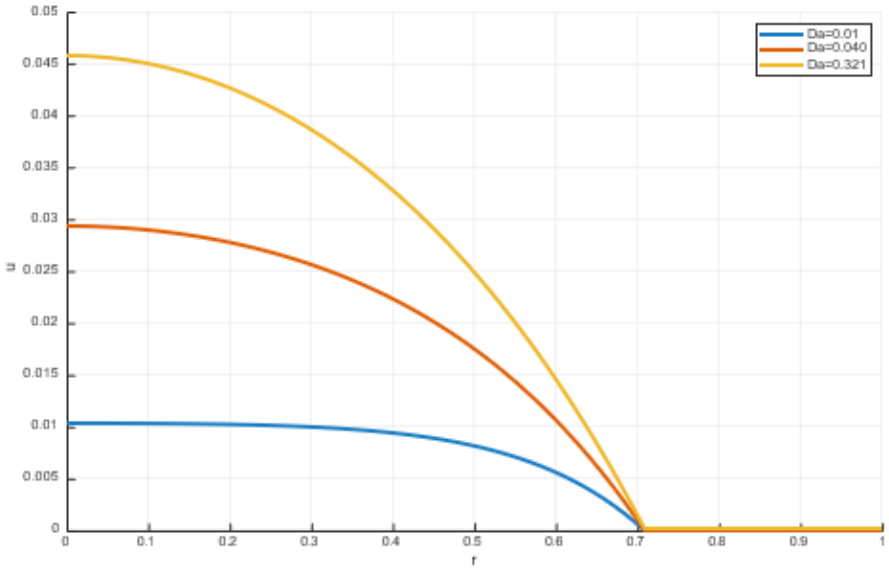

Figure 6: Axial velocity profiles with different Darcy number when needle depth is0.2 *mm*.

Conclusion

The present study develops a mathematical model of interstitial fluid flow induced by a perpendicular needle insertion at ST36 acupoint using the convective Brinkman law along with Kelvin-Voigt viscoelastic stress. The governing equations were solved with the help of an implicit finite difference scheme using cylindrical coordinates with appropriate boundary conditions, which represent precisely the tissue and needle interface.

A grid independence study was also performed on various grid sizes to ensure numerical accuracy. 50 × 100 grid was adopted as the standard mesh for all computations, which provides a balance between computational efficiency and accuracy.

The numerical results show that the fluid flow in this interstitial medium is mainly governed by permeability and pressure forcing. Variation in Reynolds number shows a slight change in velocity profiles, which indicates that the flow is in a viscous-dominated medium, which is the case of an interstitial medium. The increase in needle depth indicates a proportional increase in fluid velocity, which demonstrates the effect of pressure on fluid flow locally near the needle.

References

1. Swartz MA, Fleury ME (2007) Interstitial flow and its effects in soft tissues. Annu Rev Biomed Eng 9(1): 229-256.
2. Yao W, Li Y, Ding G (2012) Interstitial fluid flow: the mechanical environment of cells and foundation of meridians. Evid Based Complement Alternat Med 2012: 853516.
3. Langevin HM, Yandow JA (2002) Relationship of acupuncture points and meridians to connective tissue planes. Anat Rec 269(6): 257-265.
4. Yu X, Ding G, Huang H, Lin J, Yao W, Zhan R et.al (2009) Role of collagen fibers in acupuncture analgesia therapy on rats. Connect Tissue Res 50(2): 110-120.
5. Kumar S, Kumar (2023) Blood flow with heat transfer through different geometries of stenotic arteries. Trends in Sciences 20(11): 6965-6965.
6. Deleuze Y, Thiriet M, Sheu T (2015) Modeling and simulation of local physical stress on the mastocytes created by the needle manipulation during acupuncture. Communications in Computational Physics 18(4): 850-867.
7. Hall JE (2015) Guyton and Hall Textbook of medical physiology.
8. Yao W, Shen Z, Ding G (2013) Simulation of interstitial fluid flow in ligaments: comparison among Stokes, Brinkman and Darcy models. International journal of biological sciences 9(10): 1050-1056.
9. Deleuze Y, Thiriet M, Sheu TW (2016) On three-dimensional ALE finite element model for simulating deformed interstitial medium in the presence of a moving needle. Computers and Fluids 141(3): 75-81.
10. Huang H, Yue X, Huang X, Long W, Kang S, Rao Y et.al (2022) Brain activities responding to acupuncture at ST36 (zusanli) in healthy subjects: a systematic review and meta-analysis of task-based fMRI studies. Frontiers in Neurology 13: 930753.
11. Sun ZG, Pi YL, Zhang J, Wang M, Zou J, Wu W et.al (2019) Effect of acupuncture at ST36 on motor cortical excitation and inhibition. Brain and behavior 9(9): e01370.
12. Nield DA, Bejan A (2006) Convection in porous media.
13. Callejas A, Melchor J, Faris I H, Rus G (2021) Viscoelastic model characterization of human cervical tissue by torsional waves. Journal of the mechanical behavior of biomedical materials 115: 104261.
14. LoCastro E, Paudyal R, Mazaheri Y, Hatzoglou V, Oh JH, Lu Y et.al (2020) Computational modeling of interstitial fluid pressure and velocity in head and neck cancer based on dynamic contrast-enhanced magnetic resonance imaging:feasibility analysis. Tomography 6(2): 129-138.
15. Yunshan L, Chengli X, Peiming Z, Haocheng Q, Xudong L, Liming L et.al (2025) Integrative research on the mechanisms of acupuncture mechanics and interdisciplinary innovation. BioMedical Engineering OnLine 24(1): 30.
16. Han YJ, Yi SY, Lee YJ, Kim KH, Kim EJ, Lee SD et.al (2015) Quantification of the parameters of twisting–rotating acupuncture manipulation using a needle force measurement system. Integrative Medicine Research 4(2): 57-65.
17. Han P, Che D, Pallav K, Ehmann K (2012) Models of the cutting edge geometry of medical needles with applications to needle design. International Journal of Mechanical Sciences 65(1): 157-167.
18. Tang L, Du D, Yang F, Liang Z, Ning Y, Wang Het.al (2015) Preparation of graphene-modified acupuncture needle and its application in detecting neurotransmitters. Scientific reports 5(1): 11627.
19. Terzano M, Dini D, Rodriguez y BF, Spagnoli A, Oldfield M (2020) An adaptive finite element model for steerable needles. Biomechanics and Modeling in Mechanobiology 19(5): 1809-1825.